T H E U N I V E R S I T Y O F M I C H I G A N

COLLEGE OF ENGINEERING
Department of Mechanical Engineering
Heat Transfer and Thermodynamics Laboratory

Quarterly Progress Report No. 2
For the Period April through June, 1960

PRESSURIZATION OF LIQUID OXYGEN CONTAINERS

J.A. Clark
H. Merte, Jr.
W.O. Winer
V.S. Arpaci
D.F. Jankowski
M. Starr
R. B. Keller
W.A. Beckman

UMRI Project 03583

under contract with:

DEPARTMENT OF THE ARMY
DETROIT ORDNANCE DISTRICT
CONTRACT NO. DA-20-018-506-ORD-254
DETROIT, MICHIGAN

administered by:

THE UNIVERSITY OF MICHIGAN RESEARCH INSTITUTE ANN ARBOR

August 1960

TABLE OF CONTENTS

LIST OF FIGURES

ABSTRACT

The status of the new experimental system is discussed. The results of an Army Ballistic Missile Agency study have been examined and compared with those of this project.

A theoretical analysis of the dynamic response of the temperatures of the pressurizing gas and container wall has been completed and is presented. The analysis considers two modes of heat-transfer interaction between the container and the ambient: (a) convective heat transfer with an ambient at constant temperature; (b) imposed heat flux on the container wall. A container insulated from the ambient is a special case of (b). Some experimental data are compared with the analysis, generally favorably.

The experimental apparatus for the study of the boiling of a cryogenic fluid in a force field of zero and reduced gravity is under construction and is described. A preliminary analysis of the proposed transient method of measuring the heat-transfer parameter is given.

The experimental apparatus for the study of heat transfer to a cryogenic fluid in an accelerating system is under construction and is described. The orientation of the acceleration vector in the basic test vessel is normal to the heating surface, but the case with the acceleration vector parallel to the heating surface is being considered. This will require only minor additions to the test apparatus.

I. OPTIMIZATION OF PRESSURIZED-DISCHARGE PROCESSES IN CRYOGENIC CONTAINERS

A. EXPERIMENTAL PROGRAM

During the last period the new experimental system, discussed in Progress Report No. 1, May, 1960, has been under construction. It is expected to be in operation in the near future.

This new design incorporates the following features, namely; a styrofoam lining inside the top of the container, a floating thermocouple column, 220-v heaters of wound Chromel A ribbon, and an annular container to enclose the main test tank to provide a "guard-heater" type of control of the ambient. The design of the system has been completed and construction is near completion. Figure 1 shows a cutaway view of the new system. Figure 2 is a detail of the annular container. Figure 3 shows a wiring diagram for the 220-v heaters.

A U.S. Army Ballistic Missile Agency report[1] concerning pressurized-discharge processes was reviewed and the results given were compared with those of this project. Upon normalizing the residual densities to a pressure of 50 psia (a procedure used in this research), the residual density for a given inlet gas temperature showed agreement within 4% of similar experimental results obtained in this research. The University of Michigan data used in this comparison are reported in Progress Report No. 17, August, 1959.

B. ANALYSIS OF GAS- AND WALL-TEMPERATURE RESPONSE DURING THE DISCHARGE OF A CRYOGENIC LIQUID FROM A CONTAINER

During the last period the analysis of the dynamic response of the pressurized-discharge process was revised and completed. In the analysis presented previously, it was necessary to assume that the gas-wall and liquid-wall convection coefficients were equal. In the physical system they differ by a factor of ten or more and for this reason in the present study it was necessary to change the analytical model. Two separate cases are investigated.

The basic physical system analyzed is shown in Fig. 4. This consists of a cylindrical container from which the cryogenic liquid is discharged by means of a pressurizing gas.

The first case considers the container exchanging heat with the ambient through a convection heat-transfer coefficient. The second case considers an arbitrary heat flux imposed on the outer surface of the container. The proper combination of the separate parts of the analysis, which is discussed below,

provides the solution for simultaneous heat transfer with the ambient and an imposed heat flux. This combination closely approximates the conditions imposed on cryogenic containers on space vehicles where both heat transfer with the ambient and external heat flux may be expected to occur.

The following assumptions are made: (a) the velocity transient at the start of discharge of the liquid from the container is small compared to the thermal transients and therefore is neglected; (b) the axial conduction of heat is neglected in both the container wall and in the pressurizing gas; (c) the radial temperature distribution in both the container wall and the pressurizing gas are ignored, the temperature in each being lumped; (d) average convection heat-transfer coefficients are assumed to be constant; (e) physical properties of both container wall and pressurizing gas are constant; and (f) the dynamic response of the system is introduced by two sources: (i) change in the temperature of the pressurizing gas at the inlet of the container and/or (ii) the imposition of a heat-transfer interaction with the ambient. The heat-transfer interaction with the ambient consists of two separate modes: (a) heat transfer through a convection coefficient of heat transfer with an ambient at constant temperature and (b) an imposed heat flux on the outer wall of the container.

It has been observed from experimental measurements that the liquid and wall temperatures below the liquid-gas interface had a negligibly small variation during the period of the discharge of the liquid from the container. This results from the fact that the liquid is at a saturated state corresponding to the initial pressure, and acts as a heat sink at constant temperature. Futhermore, it has a very large heat capacity and has a low thermal resistance between it and the wall. Therefore, in the following analysis, heat transfer between the container and the ambient is assumed negligible for all regions below the liquid-gas interface. This is accomplished by assuming, in Case I, a constant ambient temperature equal to the liquid temperature below the liquid-gas interface, and in Case II, an imposed constant heat flux above the liquid-gas interface only. Thus, in Case I, the ambient moves with the liquid-gas interface, wetting only that part of the container wall above the interface, and in Case II, the imposed heat flux moves with the liquid-gas interface, affecting only that part of the container wall above the interface.

In both these cases the difficulty arising from assuming the same convection coefficients of heat transfer above and below the liquid-gas interface is eliminated.

The differential equations from the First Law of Thermodynamics with associated initial-boundary conditions for this system are:

For the Gas:

$$\frac{\partial T^*}{\partial \theta} + V \frac{\partial T^*}{\partial x} + b_1(T^* - t^*) = 0 \qquad (1)$$

For the container wall:

$$\frac{\partial t^*}{\partial \theta} - b_2(T^* - t^*) - \begin{Bmatrix} b_3(T_a^* - t^*) \\ \phi \end{Bmatrix} = 0 \tag{2}$$

$$T^*(x,0) = T_\ell^* \tag{3}$$

$$t^*(x,0) = T_\ell^* \tag{4}$$

$$T^*(0,\theta) = T_g^* \tag{5}$$

where T_ℓ^* is the saturated liquid temperature and T_g^* is the temperature of the pressurizing gas at the inlet to the container. In Eq. (2), $b_3(T_a^* - t^*)$ corresponds to Case I, the moving ambient, where

$$T_a^* = \begin{cases} T_a^* , & x \leqslant V\theta \\ T_\ell^* , & x > V\theta \end{cases} \tag{6}$$

and ϕ corresponds to Case II, the moving heat flux, where

$$\phi = \begin{cases} \phi , & x \leqslant V\theta \\ 0 , & x > V\theta \end{cases} \tag{7}$$

The method of analysis for both cases is essentially the same and therefore only Case I will be carried out in detail. The results of Case II will be presented.

Method of Analysis

Case I - Moving Ambient.—Upon scaling all temperatures to the saturation temperature of the liquid, the energy equations for Case I become:

$$\frac{\partial T}{\partial \theta} + V \frac{\partial T}{\partial x} + b_1(T - t) = 0 \tag{8}$$

$$\frac{\partial t}{\partial \theta} - b_2(T - t) + b_3(t - T_a) = 0 \tag{9}$$

$$T(x,0) = 0 \tag{10}$$

$$t(x,0) = 0 \tag{11}$$

$$T(0,\theta) = T_g \tag{12}$$

$$T_a = \begin{cases} T_a , & x \leqslant V\theta \\ 0 , & x > V\theta \end{cases} \tag{13}$$

For mathematical convenience only, the above problem can be separated into the following two problems in which $T = T_1 + T_2$ and $t = t_1 + t_2$.

$$\frac{\partial T_1}{\partial \theta} + V \frac{\partial T_1}{\partial x} + b_1(T_1 - t_1) = 0 \tag{14}$$

$$\frac{\partial t_1}{\partial \theta} - b_2(T_1 - t_1) + b_3(t_1 - 0) = 0 \tag{15}$$

$$T_1(x,0) = 0 \tag{16}$$

$$t_1(x,0) = 0 \tag{17}$$

$$T_1(0,\theta) = T_g \tag{18}$$

$$\frac{\partial T_2}{\partial \theta} + V \frac{\partial T_2}{\partial x} + b_1(T_2 - t_2) = 0 \tag{19}$$

$$\frac{\partial t_2}{\partial \theta} - b_2(T_2 - t_2) + b_3(t_2 - T_a) = 0 \tag{20}$$

$$T_2(x,0) = 0 \tag{21}$$

$$t_2(x,0) = 0 \tag{22}$$

$$T_2(0,\theta) = 0 \tag{23}$$

The solution of Eqs. (14)-(18) is obtained by the use of the Laplace Transformation in the timewise domain. The subsidary equation in terms of the gas temperature, T_1, is

$$\frac{d\bar{T}_1}{dx} + \frac{1}{V}\left(p + b_1 - \frac{b_1 b_2}{p+b}\right)\bar{T}_1 = 0 \tag{24}$$

with the transformed boundary condition

$$\bar{T}_1(0,p) = T_g/p \tag{25}$$

where

$$b = b_2 + b_3 \, . \tag{26}$$

The solution of the above equation is obtained directly from the methods of treating ordinary differential equations. It is

$$\frac{\bar{T}_1}{T_g} = \frac{1}{p} e^{-\frac{x}{V}p} \cdot e^{-\frac{b_1 x}{V}} \cdot e^{\frac{b_1 b_2 x}{V(p+b)}} \tag{27}$$

Combining Eq. (27) with the Laplace transformation of Eq. (15), the transformed wall temperature is found to be

$$\frac{\bar{t}_1}{T_g} = b_2 e^{-\frac{x}{V}p} \cdot e^{-\frac{b_1 x}{V}} \cdot \frac{e^{\frac{b_1 b_2 x}{V(p+b)}}}{p(p+b)} \tag{28}$$

The inverse transforms of Eqs. (27) and (28) can be obtained by the use of a table of Laplace Transforms.[2] They are

$$\frac{T_1}{T_g} = \bar{e}^{s} \left\{ \psi(\eta s, \frac{\delta}{\eta}) + \bar{e}^{\frac{\delta}{\eta}} \cdot I_o[2(s\delta)^{1/2}] \right\} \quad , \quad x \leqslant V\theta \tag{29}$$

$$\frac{t_1}{T_g} = \eta \, \bar{e}^{s} \, \psi(\eta s, \frac{\delta}{\eta}) \quad , \quad x \leqslant V\theta \tag{30}$$

where

$$\psi(\eta s, \frac{\delta}{\eta}) \equiv \int_o^{\delta/\eta} e^{-\frac{\delta^*}{\eta}} I_o[2(s\delta^*)^{1/2}] \frac{d\delta^*}{\eta} \tag{31}$$

$$s \equiv \frac{b_1 x}{V} \tag{32}$$

$$\delta \equiv b_2(\theta - \tfrac{x}{V}) \tag{33}$$

$$\eta \equiv \frac{b_2}{b_2 + b_3} \quad . \tag{34}$$

I_o designates the modified Bessel function of the first kind zero order. The function ψ, defined by Eq. (31), has been obtained and calculated previously by Rizika,[3] where it is presented in graphical form.

The solution of Eqs. (19)-(23), which is the main concern of this paper, is also obtained by the Laplace Transformation method. In this case it is convenient to use the Laplace transform in both the time and the space domains.

Taking the Laplace transformation of Eqs. (19)-(23) in the x (space) domain results in the following two transformed equations with the appropriate initial conditions

$$\frac{d\bar{T}_2}{d\theta} + Vq\bar{T}_2 + b_1(\bar{T}_2 - \bar{t}_2) = 0 \tag{35}$$

$$\frac{d\bar{t}_2}{d\theta} - b_2(\bar{T}_2 - \bar{t}_2) + b_3\bar{t}_2 - b_3 \frac{T_a}{q}(1 - e^{-V\theta q}) = 0 \tag{36}$$

$$\bar{T}_2(q,0) = 0 \tag{37}$$

$$\bar{t}_2(q,0) = 0 . \tag{38}$$

Defining

$$\Delta(x,\theta) = t_2 - T_2 , \tag{39}$$

the container wall-gas temperature difference, the transformed container wall and gas temperatures can be found in terms of Δ where $\bar{\Delta}$ is the Laplace transformed (in the x variable) temperature difference. They are

$$\bar{T}_2 = b_1 \int_0^{\theta} e^{-Vq(\theta - \theta^*)} . \bar{\Delta}(q,\theta^*)d\theta^* \tag{40}$$

$$\bar{t}_2 = \frac{T_a}{q}(1-e^{-b_3\theta}) + \frac{b_3 T_a}{q(b_3-Vq)}(e^{-b_3\theta} - e^{-Vq\theta}) - b_2 \int_0^{\theta} e^{-b_3(\theta - \theta^*)} . \bar{\Delta}(q,\theta^*)d\theta^* \tag{41}$$

Taking the double Laplace transform of Eq. (39) with respect to x and θ, and the Laplace transform of Eqs. (40)-(41) with respect to θ, and combining,

$$\bar{\bar{\Delta}} = \frac{T_a b_3}{p(p+b)\left[\frac{p}{V} + \frac{b_1}{V}\left(\frac{p+b_3}{p+b}\right) + q\right]} . \tag{42}$$

The inverse transformation of the foregoing equation with respect to x is

$$\bar{\Delta}(x,p) = \frac{T_a b_3}{p(p+b)} e^{-\left[\frac{p}{V} + \frac{b_1}{V}\left(\frac{p+b_3}{p+b}\right)\right] x} \tag{43}$$

On the other hand, the timewise Laplace transformation of the energy equation for the gas, Eq. (19), in terms of $\bar{\Delta}$ can be written as follows

$$p\bar{T}_2 + V\frac{d\bar{T}_2}{dx} - b_1\bar{\Delta} = 0 \tag{44}$$

$$\bar{T}_2(0,p) = 0 . \qquad (45)$$

Combining Eqs. (43) and (44) and solving for $\bar{T}_2(x,p)$, subjecting the solution to the boundary condition, Eq. (45), produces

$$\bar{T}_2(x,p) = \frac{T_a b_3}{p(p+b_3)} e^{-\frac{p}{V}x} - \frac{T_a b_3}{p(p+b_3)} \frac{(p+b)}{(p+b)} e^{-\frac{b_1}{V}\left(\frac{p+b_2}{p+b}\right)x} e^{-\frac{p}{V}x} . \qquad (46)$$

Using the timewise transform, if Eqs. (39) and (46) result in the transformed temperature of the container wall, as follows

$$\frac{\bar{t}(x,p)}{T_a} = \frac{b_3}{p(p+b_3)} e^{-\frac{p}{V}x} - \frac{b_2 b_3}{p(p+b_3)} e^{-\frac{p}{V}x} e^{-\frac{b_1 x}{V}} e^{\frac{\frac{b_1 b_2 x}{V(p+b)}}{(p+b)}} . \qquad (47)$$

Using Laplace transform tables[2] the inverse of Eqs. (46)-(47) are

$$\frac{T_2(x,\theta)}{T_a} = 1 - e^{-s} \cdot \psi(\eta s, \tfrac{\delta}{\eta}) - e^{(\delta - \frac{\delta}{\eta})} [1 - e^{-s} \psi(s,\delta)] , \quad x \leq V\theta \qquad (48)$$

$$\frac{t_2(x,\theta)}{T_a} = (1-\eta) + \eta[1 - e^{-s} \cdot \psi(\eta s, \tfrac{\delta}{\eta})] - e^{(\delta - \frac{\delta}{\eta})} [1 - e^{-s} \psi(s,\delta)] , \quad x \leq V\theta \qquad (49)$$

where ψ, which is defined previously, occurs with two different parameter systems (s,δ) and $(\eta s, \frac{\delta}{\eta})$.

The solution of the problem as stated at the beginning is the linear combination of T_1 and T_2, Eqs. (29) and (48), and t_1 and t_2, Eqs. (30) and (49).

Case II - Moving Heat Flux.—For the case of the moving heat flux, Eqs. (1)-(5) can be conveniently separated into the following two problems when the temperature is scaled to the saturation temperature of the liquid:

$$\frac{\partial T_1}{\partial \theta} + V\frac{\partial T_1}{\partial x} + b_1(T_1-t_1) = 0 \tag{50}$$

$$\frac{\partial t_1}{\partial \theta} - b_2(T_1-t_1) = 0 \tag{51}$$

$$T_1(x,0) = 0 \tag{52}$$

$$t_1(x,0) = 0 \tag{53}$$

$$T_1(0,\theta) = T_g \tag{54}$$

and

$$\frac{\partial T_2}{\partial \theta} + V\frac{\partial T_2}{\partial x} + b_1(T_2-t_2) = 0 \tag{55}$$

$$\frac{\partial t_2}{\partial \theta} - b_2(T_2-t_2)-\phi = 0 \tag{56}$$

$$T_2(x,0) = 0 \tag{57}$$

$$t_2(x,0) = 0 \tag{58}$$

$$T_2(0,\theta) = 0 , \tag{59}$$

where ϕ is defined in Eq. (7). Actually the solution of Eqs. (50)-(54) for T_1 and t_1 is a special case of the solution of Eqs. (14)-(18) where $b_3 = 0$ and hence $\eta = 1$. This special case has been solved.[3]

The second part, Eqs. (55)-(59) for T_2 and t_2, is solved in a manner similar to that used for solving Eqs. (19)-(23). The results are

$$\frac{T_2(x,\theta)}{\phi/b_2} = \delta + e^{-s}[\Lambda(s,\delta)-(1+\delta)\psi(s,\delta)] , \quad x \leqslant V\theta \tag{60}$$

$$\frac{t_2(x,\theta)}{\phi/b_2} = \delta + e^{-s}\,[\Lambda(s,\delta)-\delta\psi(s,\delta)]\,, \qquad x \leqslant V\theta \tag{61}$$

where δ, s, and ψ have been defined previously and

$$\Lambda(s,\delta) \equiv \int_0^{\delta} \delta^* e^{-\delta^*} I_0[2(s\delta^*)^{1/2}]d\delta^* \,. \tag{62}$$

The function $\Lambda(s,\delta)$ has been calculated and is presented in graphical form.[4]

The linear combination of Eqs. (29) and (30) with $\eta = 1$ and Eqs. (60) and (61) will yield the solution of the dynamic response of the gas and wall temperature of a pressurized container having an imposed wall heat flux.

The combination of the solutions for the moving ambient case, Eqs. (29) and (48) and Eqs. (30) and (49), Case I, and the solutions of the second part of the moving heat flux case, Eqs. (60) and (61), Case II, will provide the solution for the case in which both heat transfer with the ambient and an imposed heat flux occur.

Comparison of Theory and Experiment.— Calculations of the results of this analysis have been carried out for a configuration corresponding to the present experimental system. This consists of an aluminum (5052) container 12 in. ID with 1/8-in. wall thickness wrapped with two 1/32-in. layer of asbestos, around which chromel A heater wire is wound. The liquid nitrogen is pressurized and discharged by nitrogen gas at various inlet temperatures. The container is 3 ft long and is discharged in approximately 120 sec.

The principal purpose of this phase of the research is the determination of the final mean density of the pressurizing gas. For this reason the calculations were carried out for a fixed discharge time of 120 sec. In each case the pressurizing gas and wall temperature at the end of 120 sec are obtained as a function of distance in the container. From these, by numerical integration, the mean temperature of the pressurizing gas, and hence mean density at 50 psia, are obtained.

Because it is not possible, a priori to know the value of the convection heat-transfer coefficient between the pressurizing gas and the container wall, it is necessary to compare the results of the analysis for several values of this coefficient with the experimental data. For this comparison the normalized mean gas temperature (T/T_g) at 120 sec was plotted as a function of the convection coefficient for the case of the adiabatic container, Fig. 5. From

this a plot, (Fig. 6), of the mean density as a function of inlet gas temperature for various values of the convection coefficient was obtained. By superimposing the experimental data for the adiabatic runs on Fig. 6, it was determined that the value of the convection coefficient between the gas and wall which represents the best fit for these data is about 3 Btu/hr sq ft. On this basis all subsequent calculations are based on a gas-wall convection coefficient of 3 Btu/hr sq ft.

Figure 7 shows the final mean density as a function of inlet gas temperature for Case I from the theory, the system exchanging heat through a convection coefficient with the ambient at constant temperature. In this calculation the ambient was taken to be 80°F and the convection coefficient between the ambient and the container to be 2 Btu/hr sq ft. Experimental data from a previous report also are shown and discussed later.

Figure 8 is a plot from the theory of the final mean density vs. inlet gas temperature for Case II, heat flux imposed on the system. In this calculation the heat flux is a parameter and values for this quantity of 0 (adiabatic container), 1250, and 2200 Btu/hr sq ft have been plotted.

Figure 9 shows the corresponding wall temperatures vs. distance in the container at 120 sec for Case II, imposed heat flux on containers. Both inlet gas temperature and imposed heat flux are parameters.

An experimental check of the analysis can best be made after the new experimental system is in operation. As stated in the first Quarterly Progress Report for 1960, the present experimental data should not be expected to correlate completely with the analysis because of the incompatibility of the experiment and analysis with respect to the heat-transfer interaction between the container wall and the surroundings. The nature of this difficulty was discussed in the first Quarterly Report and is the main reason for adopting the new annular guarded tank design in the experimental system. It is anticipated from the existing data that the experimental program with no imposed heat flux might closely approximate the analysis where the exterior of the container is adiabatic. Existing experimental data corresponding to these conditions are compared with the analysis in Figs. 6, 8, and 9.

It is anticipated that during the next period the new experimental system will be operating and will yield data for all cases this analysis covers, i.e., no imposed heat flux, various levels of imposed heat flux, and heat exchange with the ambient.

II. BOILING OF A CRYOGENIC FLUID UNDER REDUCED GRAVITY

Design and construction of the various components of the reduced gravity test apparatus has been proceeding. The most critical component from the design and operational standpoint is the hydraulic buffer which is required to bring the test package to a stop smoothly in a short distance. A constant deceleration of 20 g's, which will bring the package to rest in 2 ft, was selected as a reasonable value. The maximum design mass of the test package and platform assembly is 100 lbs. With a terminal velocity of approximately 50 fps, a resisting force of 1900 lbs is required.

A sketch of the proposed buffer was included in 1960 Quarterly Progress Report No. 1. Figure 10 is an assembly drawing of the final design. Only one major departure has been made from the preliminary design, the elimination of a pre-load buffer piston. Its function was smoothly to accelerate the main buffer piston before direct contact with the load was made, by means of a heavy spring. However, the mass of the pre-load buffer piston was not significantly smaller than the main piston and the possibility of a large shock still existed. A heavy rubber bumper will be placed over the main piston in an attempt to absorb the initial impact.

A series of 39 holes drilled in the cylinder wall serves as a variable orifice configuration. The holes are located so that, as the piston descends under load, it covers the holes in a programmed sequence to maintain constant pressure within the cylinder. A light hydraulic oil will be used as the working fluid.

The buffer system will be instrumented and thoroughly tested using a dummy load prior to being placed in operation. The orifice holes are tapped so that the sizes can be varied, should adjustments in the deceleration rate be necessary.

Electrical interlock switches will be provided to insure that the buffer piston is fully extended prior to each drop. After dropping the piston will be extracted manually to its fully extended position.

The buffer assembly is bolted to a poured concrete base which also serves as an anchor for the guide wires. A framework of I-beams and channels attached to the upper building structure serves as a base from which the upper guide wires are suspended. Also attached to this framework are an electrically powered hoist, the release mechanism, and the counterweight pulleys. Care is taken to minimize the frictional and inertial influence of the pulleys when counterweights are used.

Although it is anticipated that the initial tests will be conducted under free fall conditions, consideration will be given during the next period to the retardation of the counterweight. With the use of a counterweight the terminal velocities will be smaller and the mass less than the main test platform, hence it is not expected to be a serious problem.

Figure 11 is a photograph of the upper support framework and Fig. 12 is a view of the drop area from this location.

Several different types of release mechanisms for the test platform are being studied. The main requirements for this device are that the release take place rapidly without exerting any motion to the test platform and that the instant of release be precisely known.

A potentiometer type accelerometer with a range of 0-1 g is being procured to be mounted on the test platform to measure its acceleration. It is specified by the manufacturer as having a sensitivity greater than 0.01 g and a time constant of 0.025 sec for a step change in acceleration.

The basic test platform will consist of a back-to-back E-frame weldment of aluminum I-beams, with the guide wires engaged by eyes at 3 locations. Figure 13 is a sketch of the proposed platform. The location of the test package, the guide wire eyes, the point of suspension, and the buffer pad will be completely adjustable so that the point of suspension and the buffer pad will be in line with the center of gravity of the entire assembly within the space available. Spirit levels mounted on the test platform will aid in the location of the center of gravity. The drop area is limited to a space 19-1/2 by 46 in. plan dimensions by structural members of the building, but is deemed sufficient for the scope of this research. The drop height is approximately 45 ft.

The first experimental apparatus to be installed on the test platform (Fig. 13) is shown in Fig. 14. The test sphere is held below the liquid nitrogen surface by means of a low-heat-capacity aluminum frame. The temperature of the sphere is monitored by the inserted thermocouples as shown.

Initially, the sphere will be at room temperature. Upon immersion into the pool of liquid nitrogen its temperature will follow a quenching curve as shown in Fig. 15. If, however, the system is suddenly subjected to zero gravity at time x within the nucleate boiling region, the heat-transfer rate will decrease and a shallower temperature-time curve will result, as indicated by the dotted curve.

If the internal thermal resistance of the sphere is negligible in comparison with the surface resistance, there will be no significant temperature gradient within the sphere at any given instant. A measure of the ratio of

internal thermal resistance to surface thermal resistance is given by the Biot Number $\bar{h}\, r_o/k$, where r_o is the sphere radius. With $\bar{h}\, r_o/k < 0.1$, the maximum variation of temperature within the sphere will be less than 5% of the initial temperature difference between the sphere and the fluid. By using a small sphere of high conductivity, the Biot Number will be minimized.

If a temperature gradient is present within the sphere, it will be observed through a difference in the temperatures indicated by the two thermocouples, Fig. 14. With no temperature gradient present, the heat-transfer analysis is greatly simplified since the system is then described by a single temperature. In such a case, a First-Law analysis for the sphere having a temperature-dependent heat capacity can be written as:

$$q = \frac{dH}{d\theta} = m\frac{d}{d\theta}\int_{t_o}^{t} Cp_s(t)dt = m\frac{d}{dt}\left[\int_{t_o}^{t} Cp_s(t)dt\right]\frac{dt}{d\theta} \qquad (63)$$

or

$$q = m\, Cp_s(t)\frac{dt}{d\theta} \qquad (64)$$

Since also

$$q = \bar{h}\, A_s(t_s - t_\ell) \ , \qquad (65)$$

then

$$\bar{h}\, A_s(t_s - t_\ell) = m\, Cp_s(t)\frac{dt}{d\theta} \ , \qquad (66)$$

where:

q = heat-transfer rate from sphere
H = enthalpy of sphere
m = mass of sphere
$Cp_s(t)$ = specific heat of sphere, a function of temperature
$\bar{h}$ = heat-transfer coefficient
A_s = sphere surface area
$t_s - t_\ell$ = sphere temperature - fluid temperature
θ = time

With the experimental temperature-time data (Fig. 15) and the specific heat-temperature dependence of the sphere known (Fig. 16), the magnitudes of q/A, $t_s - t_\ell$, and $\bar{h}$ can be found using Eq. (66).

An estimate of the magnitude of the sphere's temperature change during the drop time of 1.5 sec can be obtained by assuming an average $\bar{h}$ and C_p. The solution to the First Law for this case, Eq. (66), is then given by:

$$\frac{t(\theta) - t_\ell}{t_i - t_\ell} = \frac{\Delta t}{\Delta t_o} = e^{-K\theta} \tag{67}$$

Here Δt_o is the sphere-fluid temperature difference at $\theta = 0$, and K is the inverse time constant, $\bar{h} A_s/m C_p$. The temperature ratio $\Delta t/\Delta t_o$ versus time is given in Fig. 17. Thus, for example, if a 1/2-in. radius copper sphere is assumed to have an $\bar{h}$ of 200 Btu/hr-ft^2-°F, the value of K for use in the above equation is 424 hr^{-1} at 1.5 sec, $\Delta t/\Delta t_o$ will be approximately 0.84.

III. HEAT TRANSFER TO A CRYOGENIC FLUID IN AN ACCELERATING SYSTEM

Figure 18 is an assembly drawing of the test vessel to be used with a cryogenic fluid in the centrifuge apparatus shown in Fig. 19. The hardware is presently under construction and it is anticipated that assembly and preliminary testing will take place during the next reporting period.

The liquid temperature will be measured at two different levels to determine if, under acceleration, subcooling is present near the heating surface as was found in previous tests with water.

It is not conveniently possible to condense the vapor formed during the boiling process and the liquid depth will be changing with time. To coordinate the data taken with depth, a small float is to be installed in the test vessel and attached to a rod which will actuate 2 or 3 microswitches at preset levels. The microswitches will impress timing works on either a 4-channel Sanborn recorder or a 36-channel "Visicorder."

The decrease in liquid level during a run creates an additional problem. Since the mass of the rotating system varies, it is not possible to maintain balance with a counterweight of fixed mass. By using a counterweight incorporating a container filled with water, it is possible to maintain dynamic balance by discharging the water at the same rate that the liquid nitrogen is evaporated. Compressed air, connected to the counterweight through the upper hole in the shaft shown in Fig. 19, can be used for discharging the water through the lower hole. Calculations indicate that the center of gravity of the test vessel changes less than ± 0.1 in. from the full to empty condition. The counterweight geometry will be arranged to give a similar condition. Figure 20 is a sketch of the proposed counterweight.

To extend the study of the effect of acceleration on boiling of cryogenic fluids, provision is being made for installing a platinum wire heater in the test vessel to obtain heat fluxes up to the burnout point. Precise measurements of current and voltage drops across a known length of the wire will permit the calculation of heat flux and wire-surface temperature. This requires a stable d-c source of up to 30 amp on the rotating member.

Tests have shown that the carbon brush-copper slipping assembly presently installed is not suitable. The electrical d-c resistance varies during rotation and is believed due to an uncontrollable deposit formation on the slip rings. Although this variation is small the use of the platinum wire as a resistance thermometer dictates a permissible variation in current of less than 1 milliamp with a total current on the order of 25 amp.

To achieve a stable method of power transmission to the rotating assembly, two concentric channels were machined in a horizontal plexiglas piece and filled with mercury. Two 1/8-in.-diameter Armco Iron rods formed in a circle are inserted in each channel, one stationary and one rotating, to provide the necessary electrical contact. A cross section is shown in Fig. 21. Armco Iron was selected as it has low electrical resistance and is not attacked by mercury. Upon testing this assembly, it was observed that the current still was not sufficiently stable, both during rotation and nonrotation. Subsequent research has attributed this to the non-wetting characteristic of mercury on iron. It appears that, with the large passage of current, the electrical resistance of the film at the iron-mercury interface is highly unstable. The reduction of this resistance requires intimate contact between this iron and mercury (i.e., complete wetting).

Success in wetting has been achieved by plating an iron rod with zinc. The mercury and zinc form an amalgam, and upon removal of this amalgam the mercury remains in contact with the iron. This principle is now being extended to the assembly presently constructed.

Design calculations are being made for a cylindrical heater configuration wherein the acceleration vector will be parallel to the cylinder axis and heating surface. It is anticipated that the test vessel described above and under construction will be directly applicable to this particular study, requiring only the insertion of a suitably instrumented cylindrical heater into the fluid.

NOMENCLATURE

A	cross-sectional flow area, ft^2
A_o	cross-sectional area of container wall, ft^2
A_s	surface area of sphere
$b_1 = \frac{\bar{h}_g P}{\rho c A}$	, hr^{-1}
$b_2 = \frac{\bar{h}_g P}{\rho' c' A_o}$	, hr^{-1}
$b_3 = \frac{\bar{h}_o P_o}{\rho' c' A_o}$	, hr^{-1}
$b = b_2 + b_3$	, hr^{-1}
c	heat capacity of gas, Btu/lbm °F
c'	heat capacity of wall, Btu/lbm °F
$Cp_s(t)$	heat capacity of sphere, Btu/lbm °F
$\bar{h}$	sphere heat-transfer coefficient Btu/hr ft^2 °F
$\bar{h}_g$	gas space heat-transfer coefficient, Btu/hr ft^2 °F
$\bar{h}_o$	ambient heat-transfer coefficient, Btu/hr ft^2 °F
H	enthalpy of sphere, Btu
I_o	modified Bessel function of first kind zero order
K	inverse time constant, hr^{-1}
m	mass of sphere, lbm
p	inside perimeter of container, ft
p_o	outside perimeter of container, ft
p	Laplace transform variable in time
Q	heat transfer from sphere, Btu/hr
q	Laplace transform variable in space

q'' imposed heat flux on container, Bru/hr ft^2

$s = \frac{b_1 x}{V}$

$t(x,\theta)$ wall temperature, °F

$t_s - t_\ell$ sphere-fluid temperature difference, °F

$t_i - t_\ell$ initial sphere-fluid temperature difference, °F

$T(x,\theta)$ gas temperature, °F

T_ℓ, t_ℓ liquid temperature, °F

V interface velocity, ft/hr

x axial space coordinate, ft

$\delta = b_2(\theta - \frac{x}{V})$

$\Delta(x,\theta)$ wall-gas temperature difference, °F

θ time, hr

$\phi = \frac{q'' P_o}{\rho' c' A_o}$

ρ gas density, lbm/ft^3

ρ' density of container wall material, lbm/ft^3

$$\Lambda(s,\delta) = \int_o^\delta \delta^* e^{-\delta^*} I_o[2(s\delta^*)^{1/2}] d\delta^*$$

$$\psi(\eta s, \frac{\delta}{\eta}) = \int_o^{\delta/\eta} e^{-\frac{\delta^*}{\eta}} I_o[2(s\delta^*)^{1/2}] \frac{d\delta^*}{\eta}$$

$$\eta = \frac{b_2}{b_2 + b_3}$$

Superscripts

- the Laplace transform of the function with respect to either time or space.

= the Laplace transform of the function with respect to both space and time.

* temperature in degrees Fahrenheit absolute (temperatures without superscript star are scaled from the liquid temperature, T^*_ℓ).

Subscripts

a ambient temperature

g inlet gas temperature

m spatial mean value at $\theta = \frac{120}{3600}$ hr

REFERENCES

1. Orville E. Driver, LOX Tank Pressurization Investigation with GOX at Low and High Temperatures. ABMA DT-TN-48-59, 3 Sept. 1959.

2. Campbell, G. A., and Foster, R. M., Fourier Integrals, Van Nostrand Co., 1948, p 79, par. 655.1.

3. Rizika, J. W., "Thermal Lags in Flowing Incompressible Fluid Systems Containing Heat Capacitors," Trans. ASME, 78, 1407 (1956).

4. Arpaci, V. S., and Clark, J. A., "Dynamic Response of Heat Exchangers Having Internal Heat Sources - Part II," Trans. ASME, 80, 625-634 (1958).

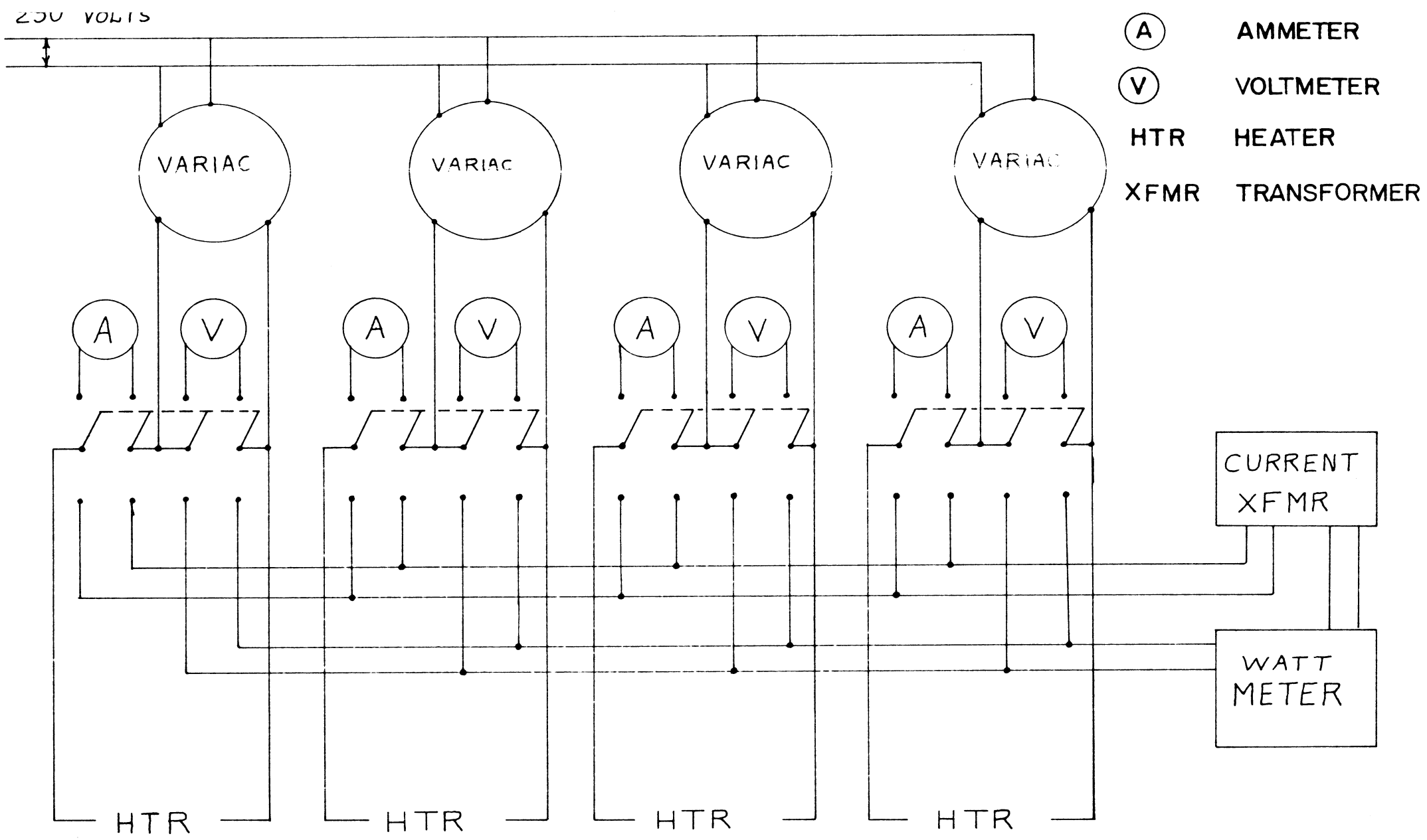

Fig.3: Resistance heating wiring diagram

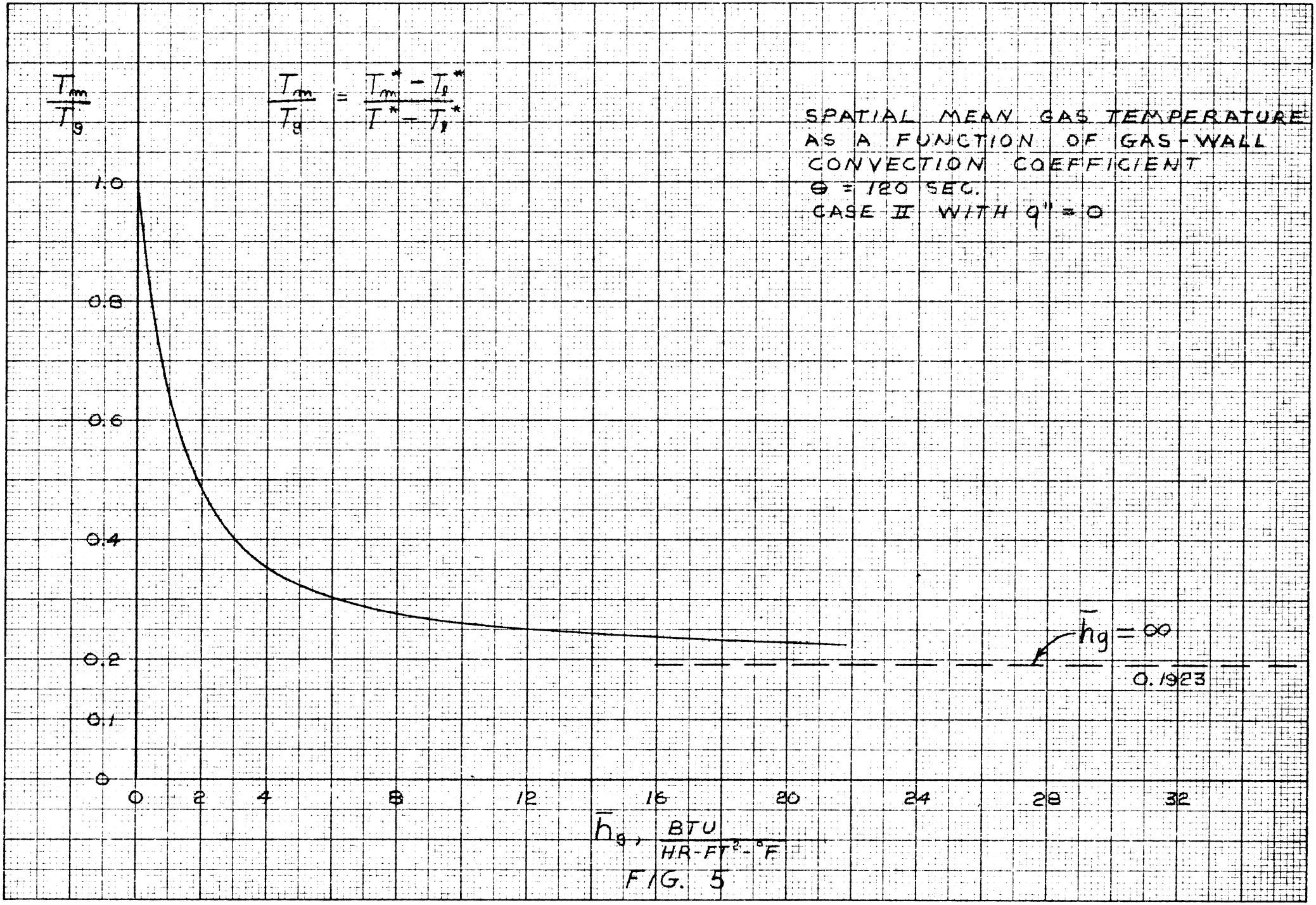
$\frac{T_m}{T_g}$
$\frac{T_m}{T_g} = \frac{T_m^* - T_f^*}{T^* - T_f^*}$
SPATIAL MEAN GAS TEMPERATURE AS A FUNCTION OF GAS-WALL CONVECTION COEFFICIENT
Θ = 120 SEC.
CASE II WITH q'' = 0
1.0
0.8
0.6
0.4
0.2
0.1
0
0
2
4
8
12
16
20
24
28
32
$\bar{h}_g = \infty$
0.1923
$\bar{h}_g$, $\frac{BTU}{HR\text{-}FT^2\text{-}^\circ F}$

FIG. 5

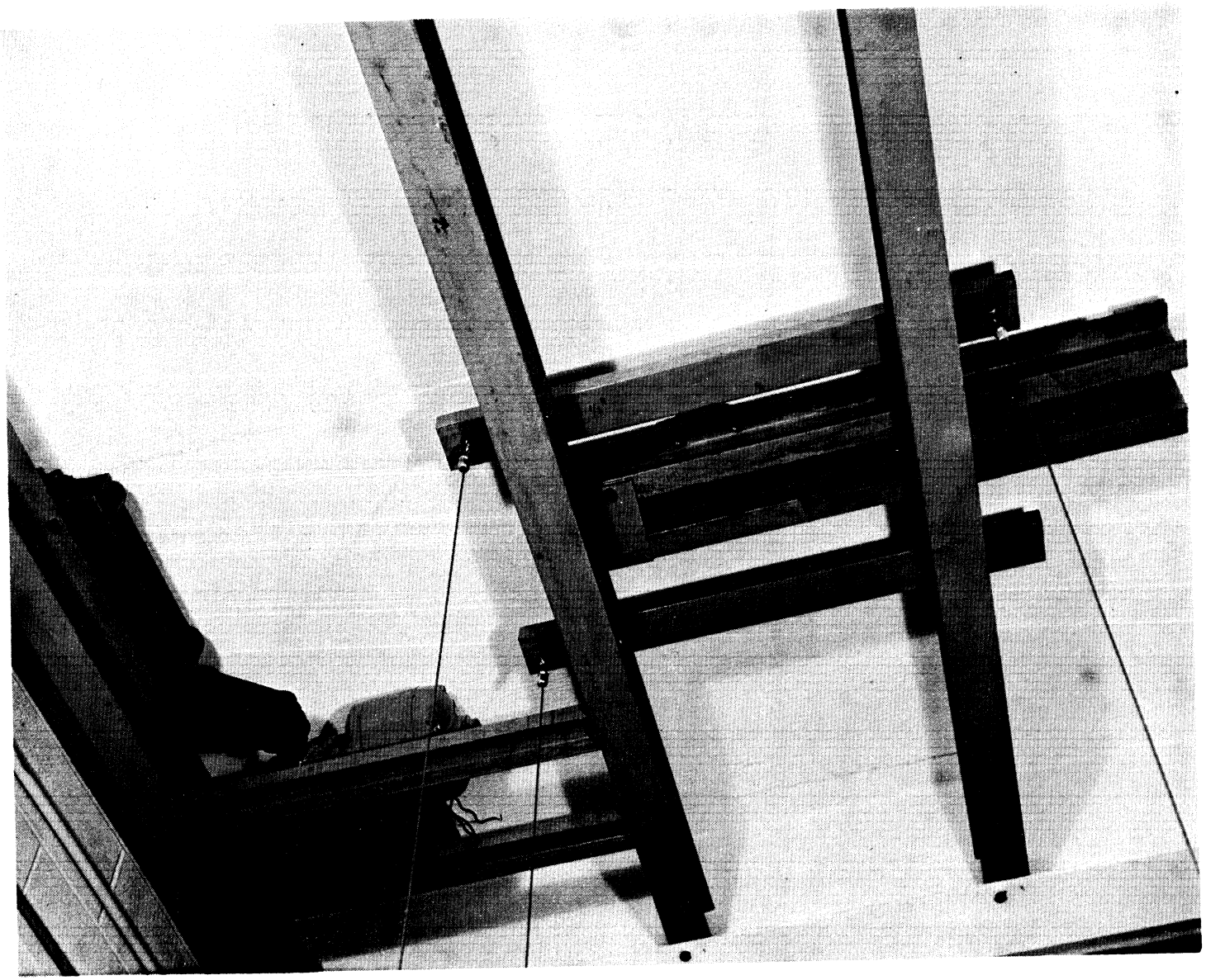

Fig. 11. Upper Support Framework for Reduced Gravity Experimental Apparatus

Fig. 12. Reduced Gravity Drop Area

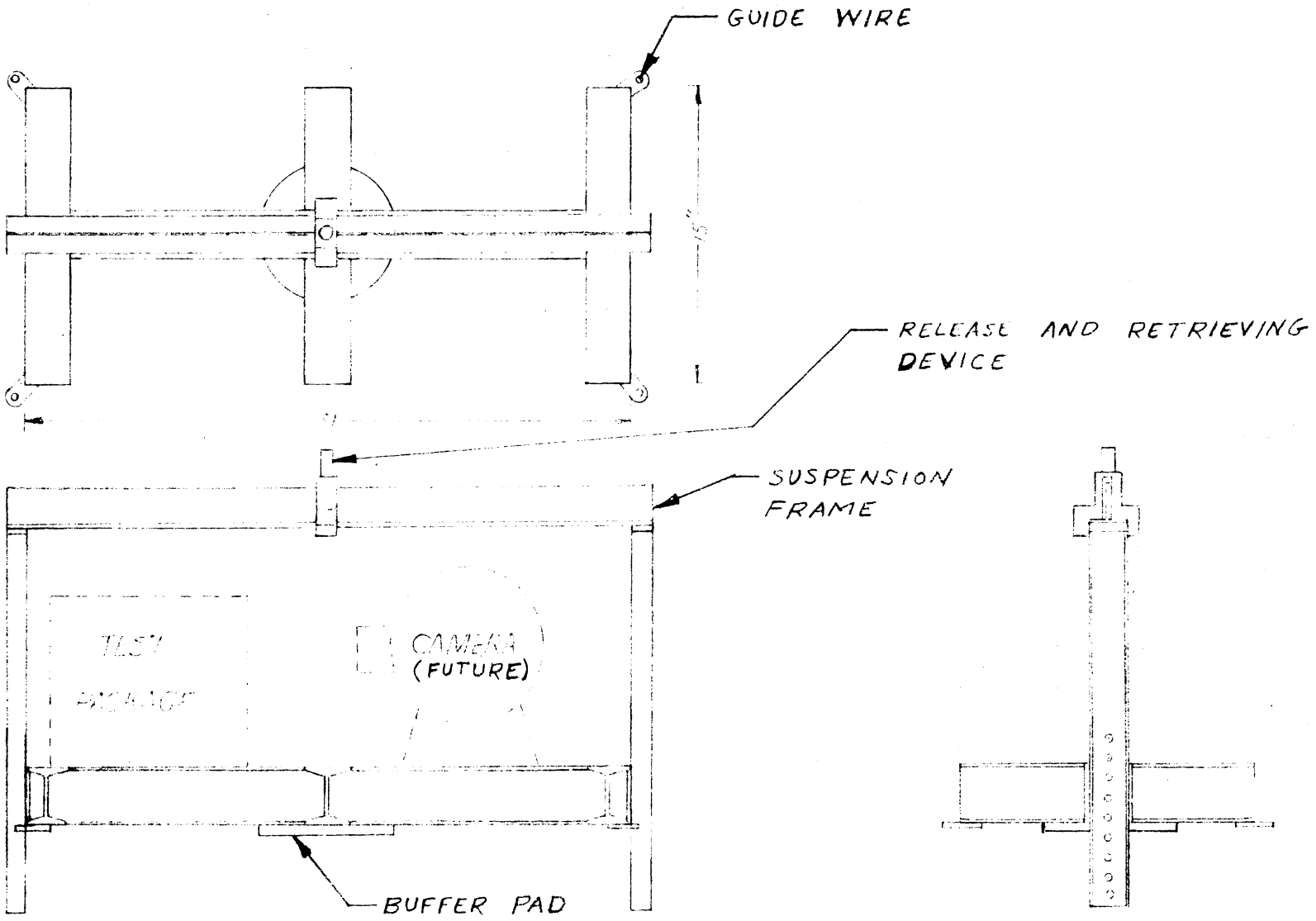

FIGURE 13. TEST PLATFORM

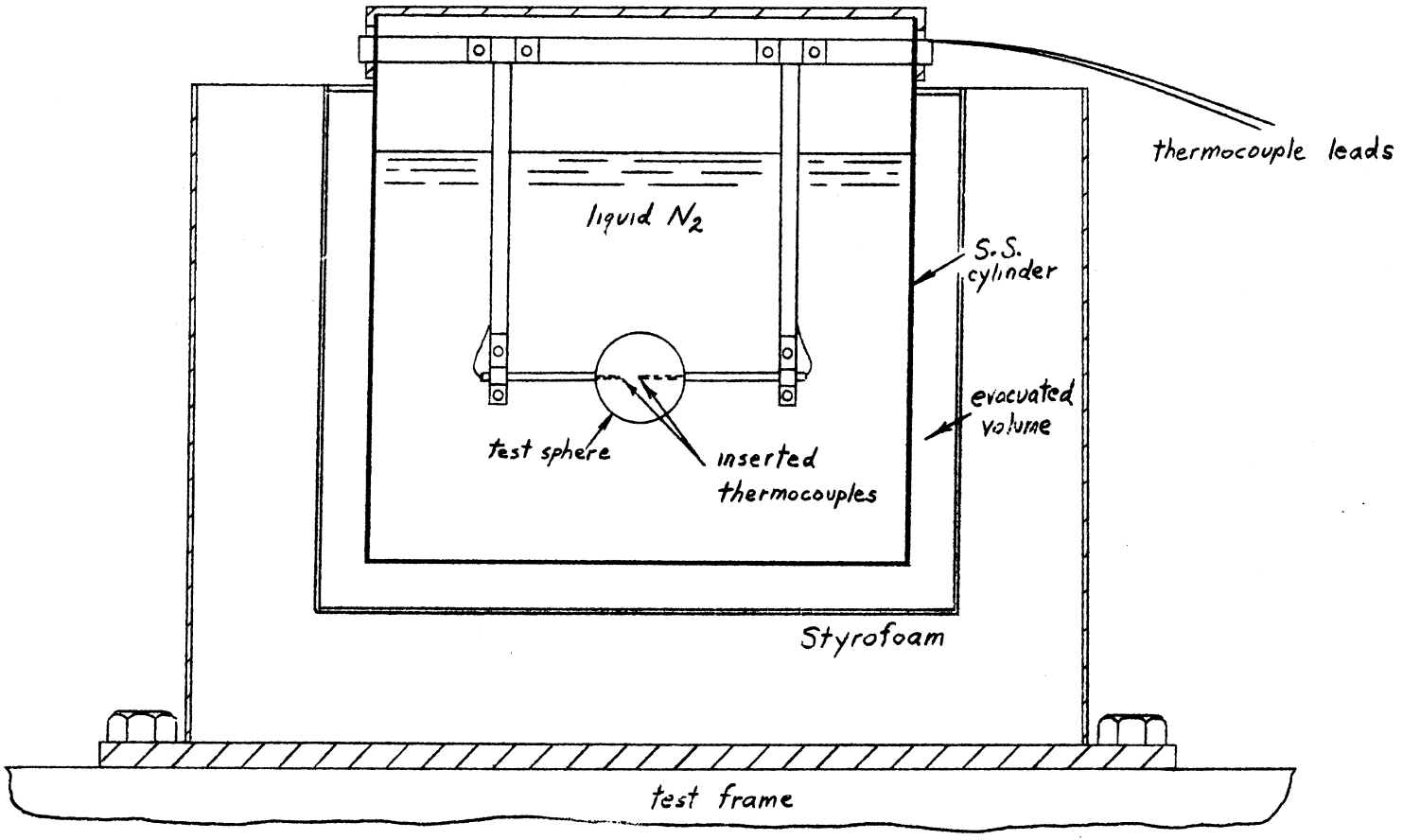

Figure 14

Reduced Gravity Test Package

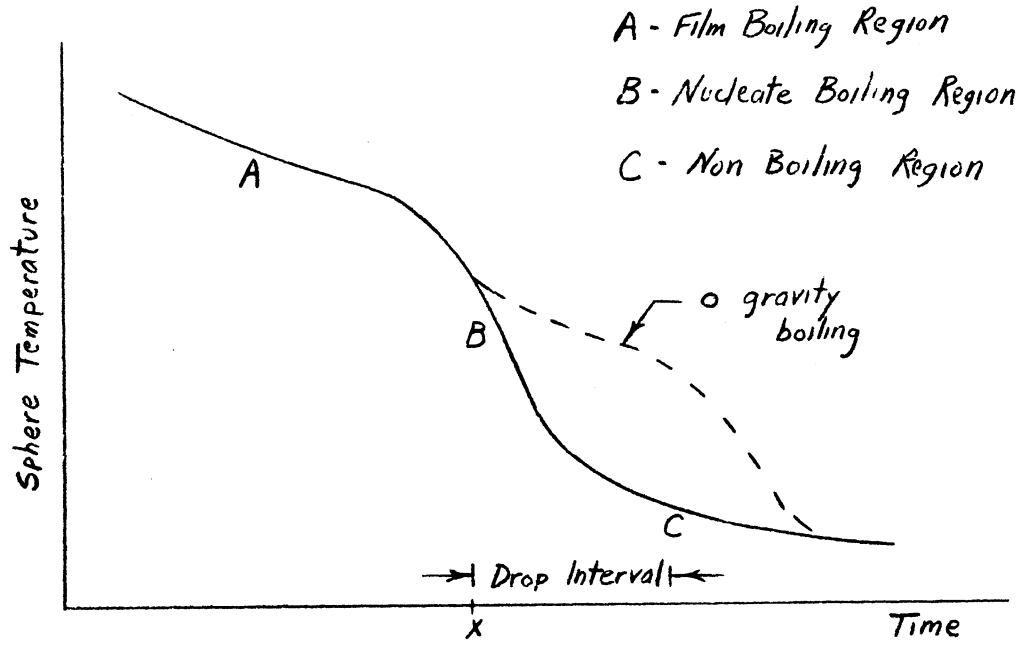

Figure 15

Anticipated Cooling Curve

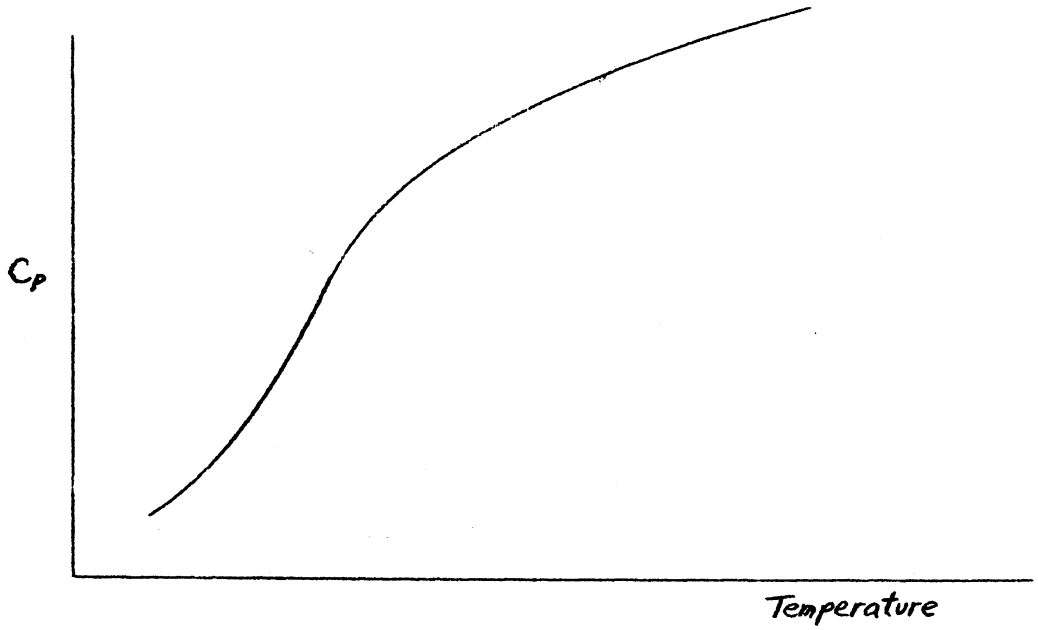

Figure 16

C_p v.s. T For Metals at Low Temperatures

Temperature Change of Sphere During Drop

$$\frac{\Delta t}{\Delta t_o} = e^{-K\theta}$$

select K from table below

Average h - BTU/hr ft² °F

	50	100	200	500
1/2" radius copper sphere	106	212	424	1060
1/2" radius aluminum sphere	184	368	736	1840

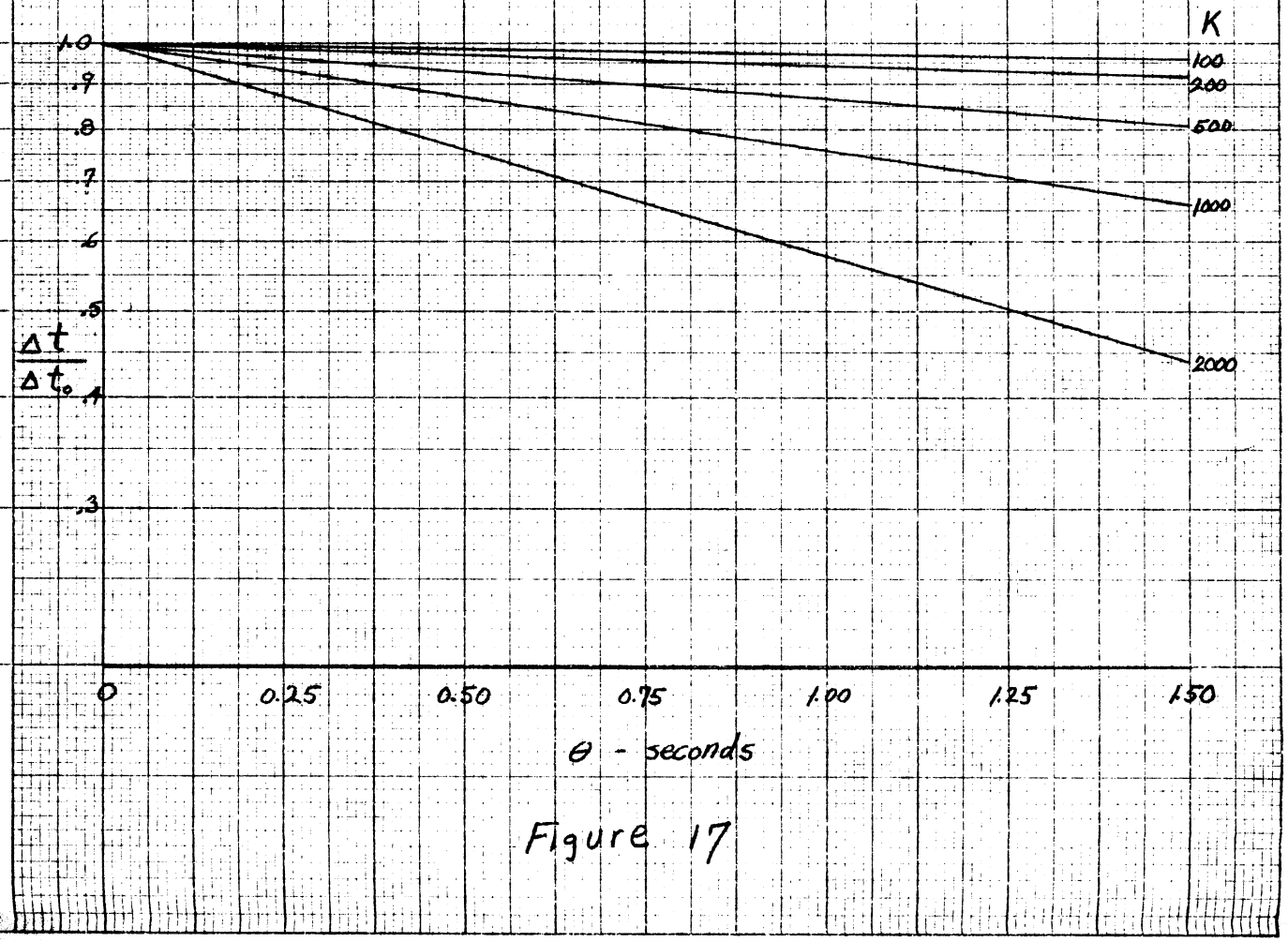

Figure 17

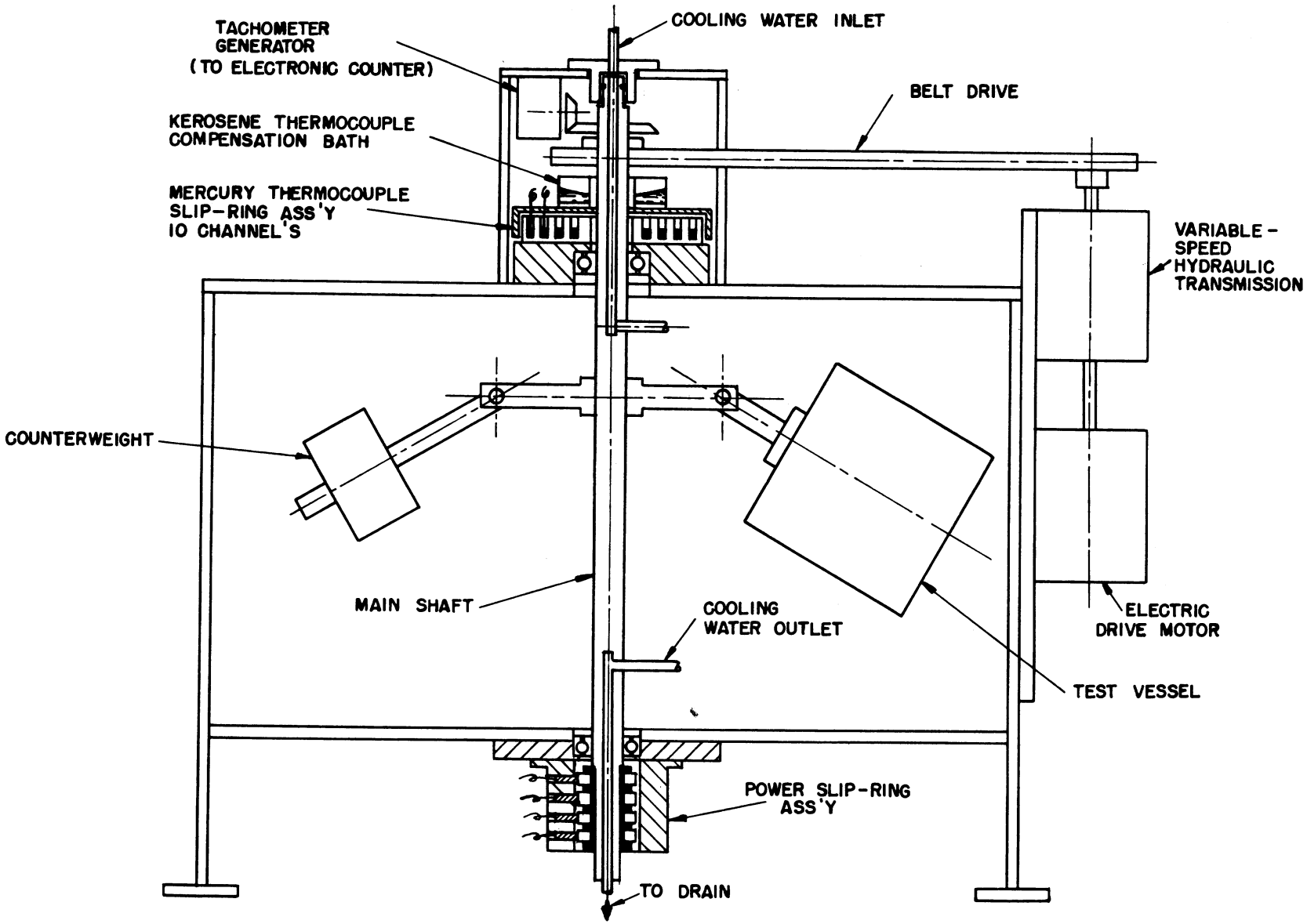

Fig. 19 Centrifuge Assembly.

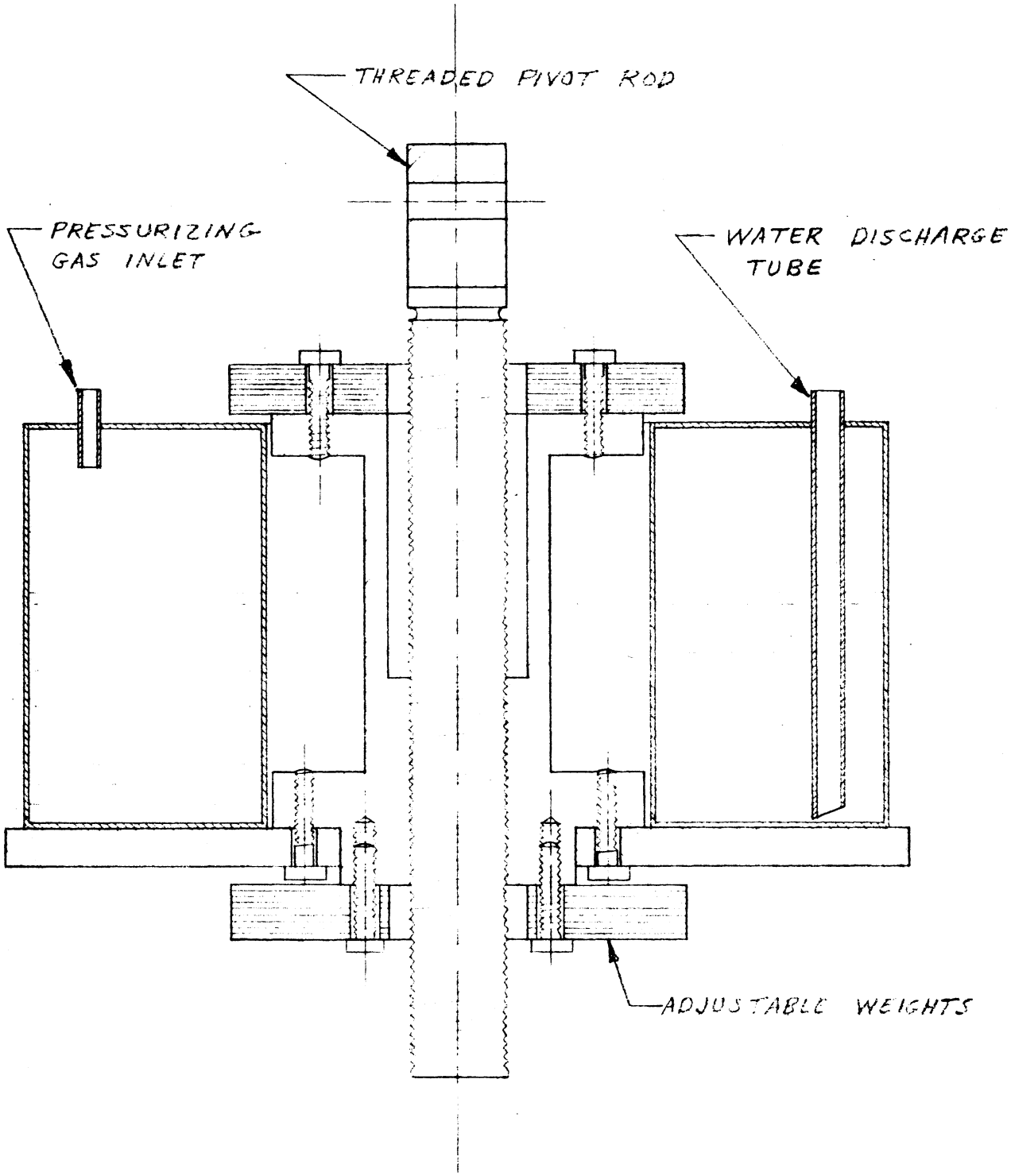

FIGURE 20. VARIABLE MASS COUNTERWEIGHT

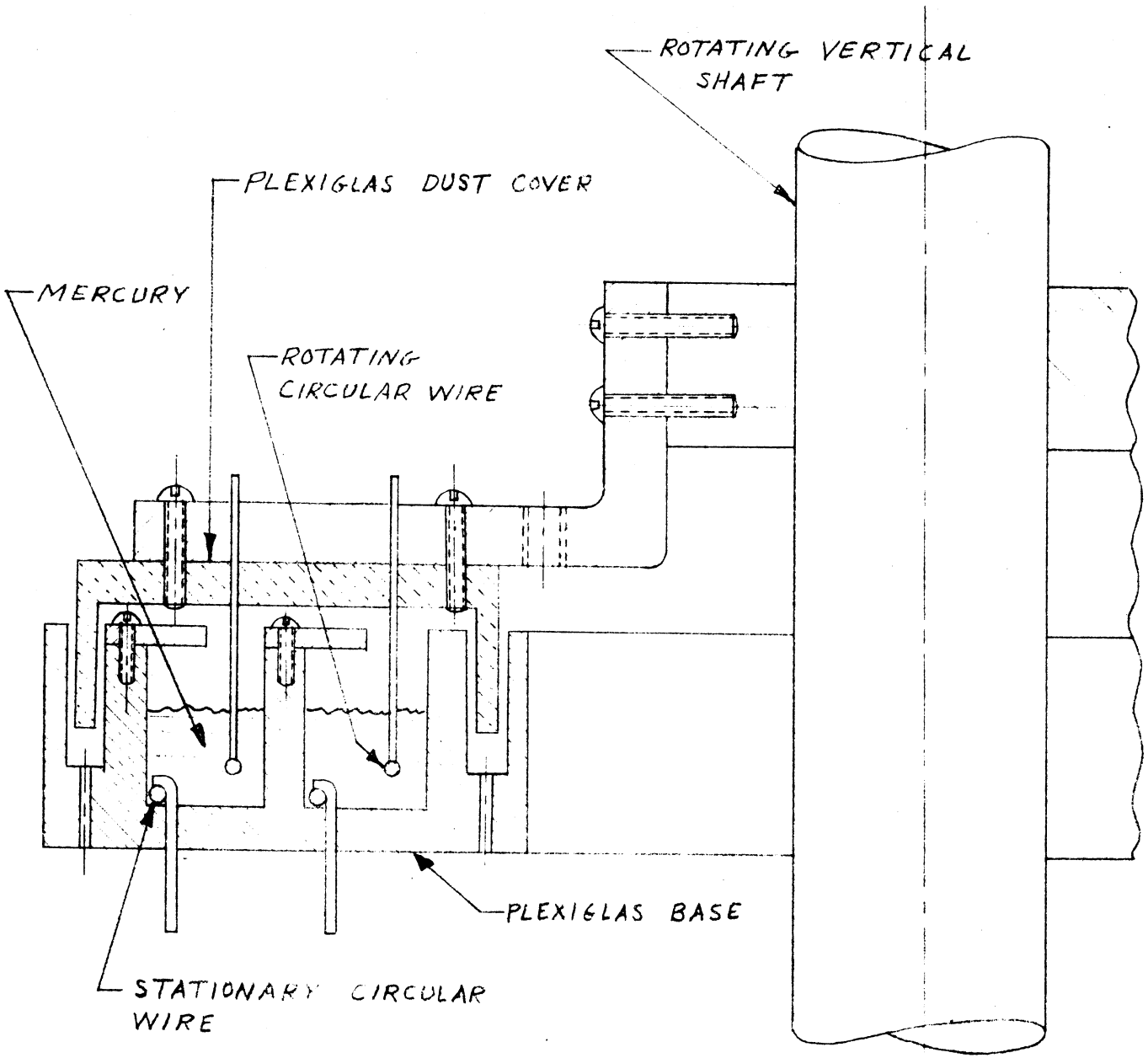

FIGURE 21. CROSS SECTION OF MERCURY D.C. POWER SLIP RING ASSEMBLY